Tapered Conical Polymer Microneedles Fabricated Using an Integrated Lens Technique for Transdermal Drug Delivery

Jung-Hwan Park, Yong-Kyu Yoon, *Member, IEEE*, Seong-O Choi, Mark R. Prausnitz*, and Mark G. Allen*, *Senior Member, IEEE*

***Abstract*—Administration of protein and DNA biotherapeutics is limited by the need for hypodermic injection. Use of micron-scale needles to deliver drugs in a minimally invasive manner provides an attractive alternative, but application of this approach is limited by the need for suitable microneedle designs and fabrication methods. To address this need, this paper presents a conical polymer microneedle design that is fabricated using a novel integrated lens technique and analyzed for its ability to insert into the skin without mechanical failure. Microneedle master structures were fabricated using microlenses etched into a glass substrate that focused light through SU-8 negative epoxy resist to produce sharply tapered structures. Microneedle replicates were fabricated out of biodegradable polymers by micromolding. Because microneedle mechanical properties are critical to their insertion into the skin, we theoretically modeled two failure modes (axial mode and transverse mode), and analytical models were compared with measured data showing general agreement. Guided by this analysis, polymer microneedles were designed and demonstrated to insert to different depths into porcine skin *in vitro*. "Long" polymer microneedles were also demonstrated in human subjects to insert deeply without failure.**

***Index Terms*—Biodegradable polymer, lens, microneedle, transdermal drug delivery.**

I. Introduction

PHARMACEUTICAL therapy is an increasingly important part of medicine; biopharmaceuticals are an increasingly important part of current drug formularies and drugs in the pipeline [1]. Unlike conventional, synthetic drugs, biopharmaceuticals such as proteins and DNA cannot be administered to patients orally and typically involve hypodermic injection, which is painful, inconvenient and requires patient training or involvement of medical personnel, especially for children and the elderly.

Transdermal drug delivery is an attractive alternative that involves transport of drugs across skin from a patch [2], [3]. Several transdermal patches have been developed for delivery of, for example, nicotine for smoking cessation and synthetic steroids for birth control, that achieve systemic medication through a topical application to the intact skin surface. Despite a number of successful patches, very few drugs can be delivered across the skin because rates of transdermal delivery are limited by the extraordinary barrier properties of the stratum corneum, the outer 10–15 μm of skin.

To address this limitation, the use of micron-scale needles was recently introduced to increase rates of transdermal drug delivery by penetrating the skin in a minimally invasive manner and thereby acting as a hybrid between hypodermic injections and transdermal patches [4]–[6]. *In vivo* delivery using such microneedles has been shown for peptides, such as insulin and desmopressin [7], [8]; genetic material, including plasmid DNA and oligonucleotides [9]; and vaccines directed against hepatitis B and anthrax [10]. Human studies have demonstrated that microneedles can be inserted into the skin without causing pain or irritation [11].

Encouraged by these drug delivery studies, microfabrication technology has been adapted to create microneedles suitable for transdermal delivery as constrained by efficacy, safety and manufacturing cost considerations. Choice of the appropriate biomaterial for microneedles is important. Although silicon has been used for many microneedle designs [12]–[14], because it is a common substrate in the microelectronics industry and, therefore, a great deal is known about its processing, silicon is relatively expensive and brittle compared to metals and polymers, involves sophisticated and expensive semiconductor processing, and has an unproven safety record in the body. Metal has been used as a more attractive alternative for microneedle fabrication [15]–[17], because it is strong, safe, and inexpensive, but fabrication of metal microneedles often requires semiconductor processes of pattering, metal deposition and electroplating. In addition, pieces of metal microneedles can be left inside skin if needle failure occurs after insertion, which may be a safety concern.

Manuscript received June 28, 2006. This work was supported in part by the National Institutes of Health. *Asterisks indicate corresponding authors.*

J.-H. Park is with Department of BioNano Technology, Kyungwon University, and the Gachon BioNano Research Institute, Gyeonggi-Do, 461-701, Korea (e-mail: pa90201@kyungwon.ac.kr).

Y.-K. Yoon was with the School of Electrical and Computer Engineering, Georgia Institute of Technology, Atlanta, GA 30332, USA. He is currently with the Electrical Engineering Department, the State University of New York at Buffalo, Buffalo, NY 14260, USA (e-mail: ykyoon@buffalo.edu).

S.-O. Choi is with the School of Electrical and Computer Engineering, Georgia Institute of Technoloy, Atlanta, GA 30332 USA (e-mail: sochoi@ece.gatech.edu).

*M. R. Prausnitz is with the School of Chemical and Biomolecular Engineering and The Wallace H. Coulter Department of Biomedical Engineering, Georgia Tech and Emory University, Georgia Institute of Technology, Atlanta, GA 30332 USA (e-mail: prausnitz@gatech.edu).

*M. G. Allen is with the School of Electrical and Computer Engineering and the School of Chemical and Biomolecular Engineering, Georgia Institute of Technology, Atlanta, GA 30332 USA (e-mail: mark.allen@ece.gaetch.edu).

Color versions of one or more of the figures in this paper are available online at http://ieeexplore.ieee.org.

Digital Object Identifier 10.1109/TBME.2006.889173

Biodegradable polymers may provide the ideal material for microneedles, given their well-known safety record and recently established ability to be fabricated by micromolding using simple methods suitable for low-cost mass production [18]. Even after breaking off in the skin by accident, or intentionally to provide controlled release of encapsulated drugs [19], biodegradable polymer needles can safely degrade in the skin.

The main disadvantage of polymer microneedles is that their relatively weak mechanical properties can cause needle failure during insertion into skin. Previous studies showed that reducing microneedle insertion force depends largely on increasing microneedle tip sharpness, while increasing microneedle failure force depends on a number of factors, including mechanical properties of the polymer, base diameter, tip diameter, height, and cross-sectional shape [18]. Given these considerations, a tapered microneedle with a wide base and a sharp tip should be a desirable geometry.

The goal of this study is to develop a process to fabricate polymer microneedles of appropriate geometry for transdermal drug delivery that can be scaled up for inexpensive mass production required for disposable drug delivery systems. Because mechanical properties are critical to the success of polymer microneedles, this study includes analytical predictions coupled with experimental measurements of microneedle failure to design polymer microneedles that do not fail upon insertion into skin. Finally, polymer microneedles were tested using porcine cadaver skin and living human subjects to determine whether they could insert into skin without failure.

II. Methods: Microneedle Fabrication and Testing

A. Fabrication of Microlenses and Microneedle Master Structures

The cost constraints of the medical device industry suggest that microneedles should cost well under US$1.00 and ideally less than US$0.10 per microneedle array when mass produced [20]. Given this constraint, a challenge of the microneedle fabrication process was not only to meet device performance benchmarks, but also to keep the fabrication process as simple as possible. The approach we took was to fabricate master microneedle structures using a one-step, lithography-based process using an integrated lens technique followed by replication by micromolding.

To fabricate microlenses, a layer of 5300 Å chromium was deposited on a glass substrate ($4 \times 4 \times 0.06$ in, sodalime glass; Telic, Palm Beach Garden, FL) and positive photoresist (AZ1518, Clariant Corp., Elgin, SC) was coated onto the chromium layer. A schematic view of the process is given in Fig. 1 [21]. The chromium layer was patterned to have a 20 by 10 array of 100-μm diameter dots with a center-to-center spacing of 400 μm in the x-direction and 800 μm in the y-direction on a glass substrate as follows. A patterned photomask was brought into contact with the photoresist on the glass substrate using an optical mask aligner (Hybralign Series 500; OAI: Optical Associates, Inc., San Jose, CA) and the photoresist was exposed to UV light (~200 mJ energy) through the photomask. The exposed photoresist was then removed by soaking in a developer (AZ 400K developer; Clariant Corp.) for 1 min. The unprotected chrome layer was etched using a chrome etchant (CR-75; Cyantek, Fremont, CA), which left behind a 20 by 10 array of holes in the chrome mask, having the geometry transferred from the photomask.

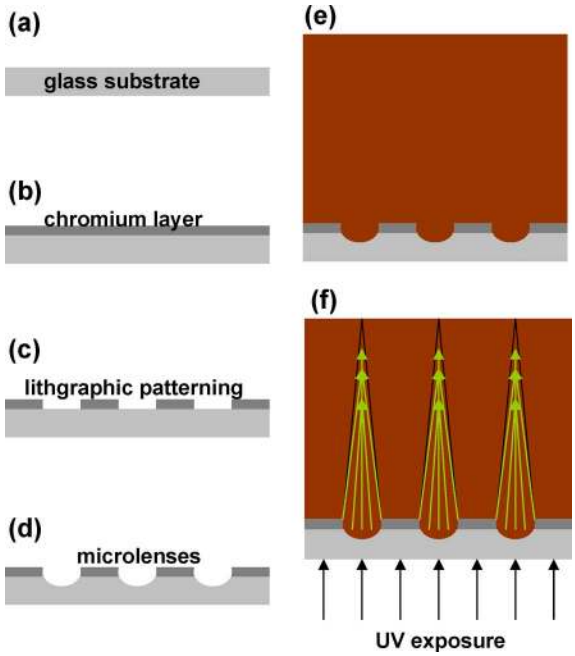

Fig. 1. Integrated lens technique fabrication sequence to make polymer microneedles. (a) A sodalime glass substrate has (b) a chromium layer deposited on its surface, which is (c) lithographically patterned and (d) etched to form hemispherical depressions that act as microlenses. After (e) coating with SU-8 negative epoxy resist, (f) UV (365 nm) exposure focuses light into a conical path that, after development, produces tapered microneedles.

Subsequently, the back side of the glass mask was coated with photoresist (1827, Shipley, Marborough, MA) to protect it from HF-HCl etching. Isotropic wet chemical etching of the glass was then performed to create a pattern of concave depressions on the front side of the glass substrate beneath each hole in the chrome mask. This was done by placing the structure in a HF-HCl solution (5% Buffered Oxide Etchant, 10% HCL, 85% D. I. Water; Aldrich Chemical Co., St. Louis, MO) at room temperature for 3 h. inisotropic etch times can result in significant lateral underetch of the chromium and subsequent chromium overhang. The resulting overhang was either removed (by a blast of nitrogen gas at 200 kPa) or left in place to control the light which passed through the original opening area in the chromium.

Casting of SU-8 negative epoxy photoresist (SU-8 100, MicroChem, Newton, MA) on this nonplanar surface resulted in a 700-μm thick film on the substrate with underlying integrated microlenses within the concave depressions, due to the refractive index difference between glass and SU-8. After 12 h of soft-baking on a 100 °C hotplate, the film was exposed from the bottom (through the glass) using UV light (7000 mJ; OAI). Due to the chromium layer on the glass, the substrate was opaque except in the microlens regions. The light passed through the lens areas to give latent images in the SU-8. Next, to cross-link the SU-8, the sample was post-baked on a hotplate for 30 min at 100 °C. After cooling, the noncrosslinked SU-8 was developed with

PGMEA (Aldrich), which yielded an array of conically tapered microneedle structures made of SU-8. The glass mask with microlenses could be reused by mechanically removing the array of SU-8 microneedle master structures from the glass substrate.

B. Fabrication of Biodegradable Polymer Microneedles

Biodegradable polymer microneedles were fabricated using polydimethylsiloxane (PDMS) molds that were made from the tapered SU-8 master structures [18]. PDMS (Sylgard 184, Dow Corning, Midland, MI) was poured over the SU-8 master structure and cured by placing in a 40 °C incubator for 12 h. The cured PDMS mold was then peeled off from the master. The SU-8 master structure could then be reused to make additional PDMS molds, although sometimes (<10% of the time), removal of the PDMS mold damaged the master structure. The PDMS mold was then filled with biocompatible polymer pellets. The biodegradable polymers that were used include poly-L-lactic acid (L-PLA, 1.1–1.3 dL/g), poly-glycolic acid (PGA, 1.4–1.8 dl/g), and poly-lactic-co-glycolic acid (PLGA, 0.5 dL/g, 1.2 dL/g) (BPI, Birmingham, AL). The polymer pellets were melted under −70 kPa vacuum for 5 min at 145 °C, 180 °C, and 230 °C for PLGA, PLA, and PGA, respectively. After cooling and solidification, the polymer microneedles were removed from the PDMS mold. The PDMS molds could then be reused to make additional polymer microneedles. We have reused PDMS molds more than 100 times, although we observed that the high temperature of melting PGA above 220 °C reduces the mold's lifetime due to PDMS degradation.

C. Measurement of Microneedle Failure Force

To measure the force that a microneedle can withstand before failure under an axial load, we used a displacement-force test station (Model 921A, Tricor System, Elgin, IL), as described previously [18]. Stress-versus-strain curves were generated by measuring force and displacement while the test station pressed an array of microneedles against a metal surface at a rate of 1.1 mm/s. Upon needle failure, the force suddenly dropped; the maximum force applied immediately before dropping was interpreted as the force of needle failure. Needles were examined by microscopy (IX-70, Olympus, Melville, NY) to validate this interpretation.

The failure force by a transverse load was also measured using the force-displacement station, as described previously [18]. A row of 5 to 10 microneedles was mounted vertically on a metal plate and a PDMS structure was pressed perpendicular to the microneedle axis against a 500 μm length of the microneedle shaft starting at the needle tip. Needle force and displacement were continuously measured until the needles were broken, as verified by microscopy.

D. Measurement of Microneedle Force of Insertion Into Skin

The relationship between insertion force and needle geometry was characterized to optimize polymer microneedles for reliable insertion into skin. The microneedle insertion force was measured as described previously [22] using the displacement-force test station. The test station continuously measured the force applied to the microneedle pressing against the skin on the hand of a human subject and measured the electrical resistance of the skin between the microneedle and the counter electrode. Because the electrical resistance of the skin's outer layer of stratum corneum is much greater than deeper tissues [23], skin resistance dropped significantly when the needle penetrated the skin. The force of insertion was interpreted as the force applied to the needle when the skin resistance dropped. Because our polymer needles were not conductive, a 0.2 μm-thick copper strip was deposited on the needle to provide a conductive pathway by DC sputtering (601 Sputtering System; CVC Products, Rochester, NY). These studies have been approved by the Georgia Tech Institutional Review Board.

E. Imaging of Microneedle Insertion Into Skin

As a simple model of transdermal drug delivery, trypan blue dye (Sigma-Aldrich) was applied to the surface of porcine cadaver skin and L-PLA microneedle arrays containing needles of 350 μm or 750 μm length were pierced into the skin and then removed. The skin specimen was immersed in a freezing block filled with Tissue-Tek Optimal Cutting Temperature solution (Sakura Finetechnical Co. Ltd, Tokyo, Japan), which was repeatedly contacted with a liquid nitrogen bath (for 5 s increments) until it was frozen. After storage in a −70 °C freezer, the frozen block was sectioned by cryostat microtome (HM 560, Microm, Walldorf, Germany) and sections of the block were examined by brightfield microscopy (IX-70, Olympus) to image the trypan blue distribution in the skin.

To assess the use of polymer microneedles in human subjects, an array of 200 PGA microneedles, all 1.5 mm in length, was manually inserted into the skin on the finger of a human subject. After removing the microneedles, evidence of microneedle insertion was analyzed by looking for blood extraction onto the skin surface by brightfield microscopy (IX-70, Olympus).

III. Results and Discussion

A. Microneedle Master Structures Fabricated Using an Integrated Lens Technique

The goal of this study was to develop a process to fabricate polymer microneedles that meet the safety, efficacy and financial constraints for transdermal drug delivery applications. Safety was addressed primarily by making microneedles out of biodegradable polymers with an established safety record with the FDA. Efficacy was addressed primarily by designing microneedles with sharp tips and sufficient mechanical strength to penetrate skin without breaking. Financial constraints were addressed primarily by developing a simple and versatile fabrication technique.

Our approach to fabrication involved first developing a method to create microneedle structures by a single step process that could easily be varied to produce sharp-tipped microneedles of different geometries. Using these master structures, biodegradable polymer microneedles could be replicated by micromolding.

To create microneedle master structures with different geometries by a single step process, we developed a fabrication method called the integrated lens technique. For this method, an array of hemispherical cavities is etched into a glass substrate covered with a chromium mask. Covering the surface with

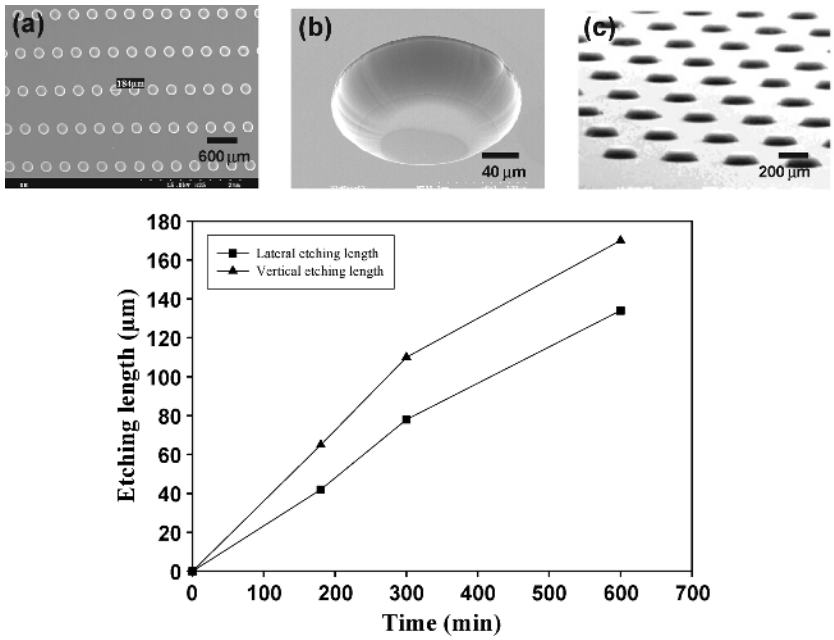

Fig. 2. Etching of microlenses. A portion of an array of microlenses etched into a glass substrate shown at (a) low and (b) high magnification; and (c) an array of PDMS mold replicas copied from the microlens array imaged by scanning electron microscopy. (d) Lateral and vertical etching length showing the resulting diameter and depth of the microlens, respectively, during etching through a chromium mask of 100-μm diameter.

a layer of SU-8 negative epoxy photoresist created integrated lenses formed by the refractive index mismatch of the SU-8 filling the cavities in the glass substrate. In this way, microneedles were formed by a single step of exposing the SU-8 to UV light from the backside, which was focused through the SU-8 layer as a tapered cone of light, after which the SU-8 was developed. Various geometries of microneedles were fabricated by changing the focal length, which was accomplished using varied lens diameters and lens opening sizes to alter the light path.

To describe this fabrication process in more detail, Fig. 2(a) and (b) shows examples of lenses etched by a HF-based etchant for 3 h. To clarify the shape of the lenses, a PDMS copy of the lens array was made and is shown in Fig. 2(c). The resultant hemispherical, concave holes have a 200-μm diameter, 70-μm depth, and center-to-center spacing of 400 μm between structures. HF-based etches usually result in a rough surface, but the recipe used in this study consisting of 10% HCl, 5% Buffered Oxide Etchant, and 85% D. I. water provides a smooth surface [24].

Microlens diameters depended on etching times, as shown in Fig. 2(d). The lateral and vertical etching rates were approximately 0.28 μm/ min and 0.39 μm/ min, respectively. When preparing microlenses, we also observed that long isotropic etch times can result in significant lateral underetch of the chromium; subsequent removal of the chromium overhang resulted in structures with wider bottoms and increased angles. Longer etching times also yielded larger radii of curvature, which resulted in structures with longer focal lengths, as expected.

Using different microlenses, microneedles with different geometries were formed. As a "control" experiment, UV light was exposed through a flat glass surface, i.e., without lenses, to produce straight columns with 500-μm length and 100-μm diameter, as shown in Fig. 3(a). Exposure through microlenses with 200-μm diameter produces microneedles measuring 980 μm in length and 26 μm at their tips, as shown in Fig. 3(b). Use of 300 μm diameter lenses produced microneedles measuring 750 μm in length and 150 μm at their tips, as shown in Fig. 3(c). Use of a 390-μm lens diameter created microneedles measuring 1070 μm in length and 120 μm at their tips, as shown in Fig. 3(d). In all cases, the needles were positioned in a 20 by 10 array with a center-to-center spacing of 400 and 800 μm. An entire array occupied an area of 9 mm by 9 mm.

Another fabrication parameter that can be used to control microneedle geometry is the presence or removal of the overhanging chromium layer created after long etching times. Fig. 4(a) shows microlenses with the overhanging chromium layer remaining; Fig. 4(b) shows the resulting microneedles, which measure 1200 μm in length, 100 μm at their bases, and about 5 μm at their tips. If the overhanging chromium layer is removed, the microneedles are 1000 μm in length, 250 μm at their bases, and approximately 20 μm at their tips, as shown in Fig. 4(c). This demonstrates how an oversized (i.e., underetched) lens combined with an overhanging mask can be used to produce high aspect ratio microneedles with very sharp tips.

B. Analysis of Microneedle Geometry Produced by Integrated Lens Technique

To better understand and predict the patterns produced by exposure through integrated microlenses and thereby control microneedle geometry, a simulation was performed using a standard optical ray tracing simulator (IME software, Australia). For this simulation, the refractive indices of SU-8 and glass were 1.7 and 1.51, respectively. The light source used was 365-nm wavelength (i-line). The radius of curvature for the microlens

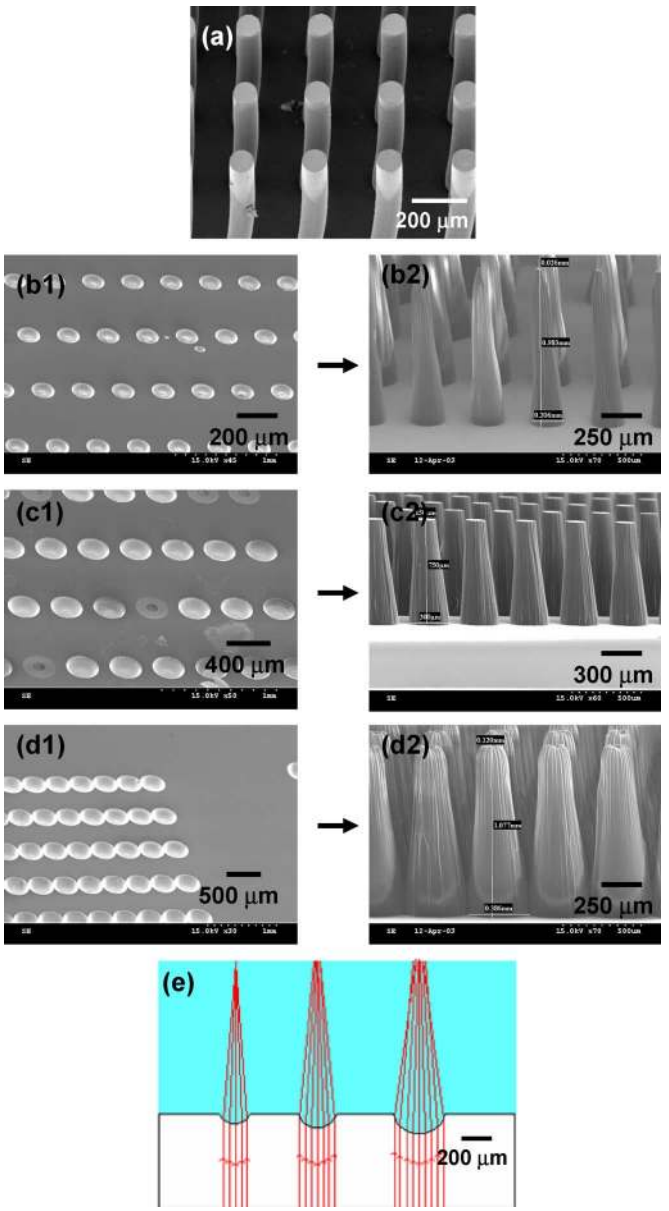

Fig. 3. Microneedle master structures produced by the integrated lens technique. (a) SU-8 columns produced by UV exposure through glass without microlenses. Arrays of microlenses having (b1) 200 μm, (c1) 300 μm, and (d1) 400 μm diameter. Arrays of SU-8 microneedle master structures produced using microlenses of (b2) 200, (c2) 300, and (d2) 400 μm diameter. All images were produced by scanning electron microscopy. (e) Ray-tracing simulation with lens diameters of 200, 300, and 400 μm, shown from left to right, respectively.

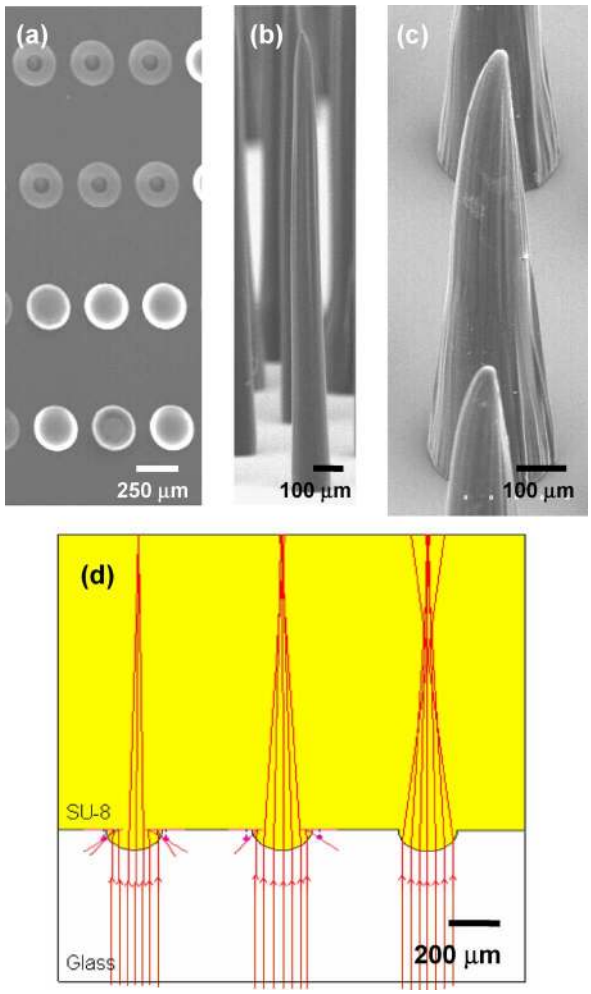

Fig. 4. Microneedle master structures produced by varying the chromium layer overhanging the microlens. (a) An array of microlenses covered by an overhanging chromium layer with 100-μm diameter opening holes. (b) SU-8 microneedles with 5-μm tip diameter, 100-μm base diameter, and 1200-μm length produced using the microlenses shown in (a). (c) SU-8 microneedles with 20-μm tip diameter, 250-μm base diameter, and 1000-μm length produced using the microlenses shown in (a) with the chromium overhang removed. All images were produced by scanning electron microscopy. (d) Ray-tracing simulation with different amounts of chromium layer overhang corresponding to 100-, 150-, and 200-μm diameter opening holes shown from left to right.

was 100 μm. Simulation results for varying lens opening diameters of 200 μm, 300 μm, and 400 μm are presented from left to right in Fig. 3(e). To compare simulation results to the actual structures, the cross-sectional diameters at a height of 500 μm from the bottom of SU-8 microneedles were measured by scanning electron microscopy to be 150 μm, 206 μm, and 293 μm for exposure through lens opening diameters of 200 μm, 300 μm, and 400 μm, respectively. When the measured data were compared with predicted values from simulation—166 μm, 237 μm, and 330 μm respectively—the deviation from the measured values represented a 10%–15% overprediction.

Another parameter to control the light path is the lens opening created by an overhanging chromium layer. Simulation of an intact, partially removed, and fully removed chromium layer overhang is shown from left to right in Fig. 4(d). If the overhanging chromium is not removed, simulation predicted a 1200 μm focal length (i.e., microneedle height), which is in exact agreement with the actual structure height Fig. 4(b). If the overhanging chromium is removed, simulation predicted a 1100-μm height, which is in close agreement with the experimental value of 1000 μm Fig. 4(c).

C. Polymer Microneedle Fabrication Using Micromolding

Although SU-8 microneedles generated by the integrated lens technique could possibly be used directly for transdermal drug delivery, micromolding replicates using biodegradable polymers was preferable for increased safety and reduced

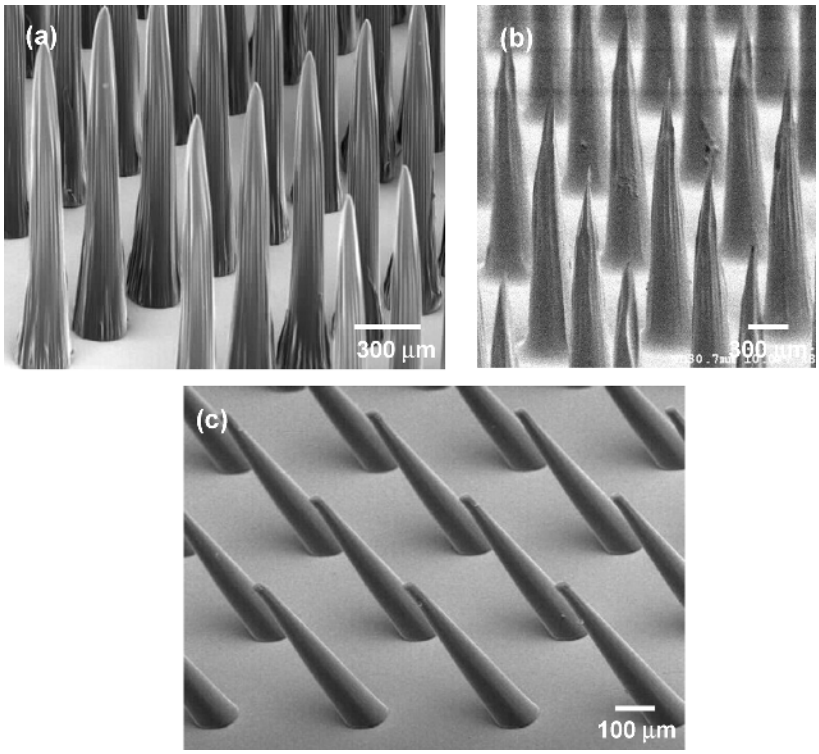

Fig. 5. Biodegradable polymer microneedles produced by micromolding microneedle master structures. (a) PGA microneedles with a base diameter of 250 μm, tip diameter of 10 μm, and length of 1500 μm. (b) PLA microneedles with a base diameter of 150 μm, tip diameter of 5 μm, and length of 75 μm. (c) Tilted PLGA microneedles with a base diameter 100 μm, tip diameter of 30 μm, and length of 400 μm oriented at an angle of 65°relative to the base substrate. All images were produced by scanning electron microscopy.

cost. As shown in Fig. 5, various geometries of biodegradable microneedles were fabricated from different kinds of biodegradable polymers to show the versatility of the fabrication method. Fig. 5(a) shows an array of 200 microneedles made of PGA, in which each needle has a base diameter of 250 μm, a tip diameter of approximately 20 μm, and a length of 1500 μm. Fig. 5(b) shows an array of 200 microneedles made of L-PLA measuring 150 μm in base diameter, 10 μm in tip diameter, and 750 μm in length. Fig. 5(c) shows an array of inclined microneedles made of PLGA with a base diameter of 100 μm, a tip diameter of 30 μm, a length of 400 μm and a 65° inclination. This array was copied from a SU-8 structure fabricated by exposure at a 45° angle from the plane of the substrate through microlenses with overhanging chromium [25]. These inclined microstructures were designed to be used to fabricate needles that can be intentionally sheared off within the skin after insertion. This might be useful for biodegradable microneedles that encapsulate drug for slow release within the skin [19].

Overall, the methods developed in this study should be especially useful to make microneedles for transdermal drug delivery, as well as other tapered microstructures for other applications. Polymer microneedle structures with high aspect ratios have been difficult to make using previous fabrication methods. The combination of the integrated lens technique and micromolding provides a simplified process to create tapered microstructures with high aspect ratios.

D. Mechanical Analysis of Insertion Force of Polymer Microneedles Into Human Skin

The efficacy of microneedles relies on sufficient mechanical strength to piece into skin. To design microneedles that penetrate skin reliably, we seek to maximize the ratio of the failure force to the insertion force. We have, therefore, measured these forces as a function of microneedle properties and have developed companion theoretical analysis.

The insertion force of polymer microneedles was measured using a force-displacement meter during penetration of microneedles into the skin of human subjects. Skin penetration was identified by a sudden drop in skin electrical resistance. Theoretical analysis of membrane penetration mechanics indicates that insertion force should depend strongly, and linearly, on the interfacial area of contact between the microneedle and skin (i.e., tip sharpness) [22]. For this reason, we measured insertion force for 20-, 50-, 64-, and 80-μm diameter microneedles, which corresponded to interfacial areas between 314 and 5000 $\mu\mathrm{m}^2$.

The resulting data are shown in Fig. 6, which can be expressed by a best-fit linear regression $(\mathrm{r}^2 = 0.747)$

$$F_i(N) = 0.00012 \times A(\mu\mathrm{m}^2) \tag{1}$$

where $\mathrm{F_i}$ is the insertion force in Newtons and A is the cross-sectional area of the microneedle tip in units of $\mu\mathrm{m}^2$. This linear

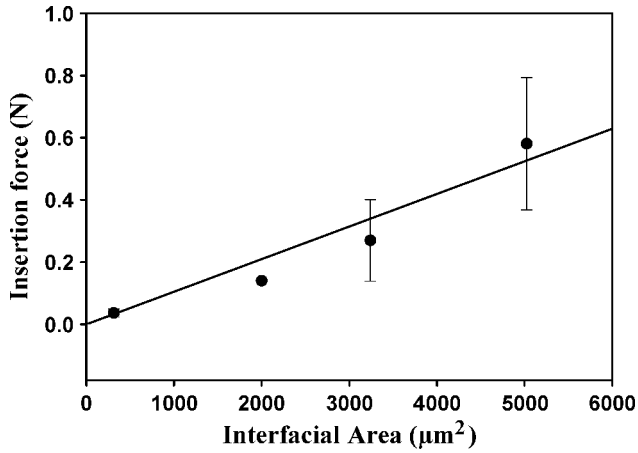

Fig. 6. Relationship between microneedle tip area and insertion force into the skin of a human subject. Insertion force increased linearly with microneedle interfacial area. This experiment used single microneedle made of L-PLA, with a base diameter of 250 μm, a length of 1000 μm, and a tip diameter that varied from 20 to 80 μm. Mean values and standard deviation error bars are shown from n = 3 replicate experiments. The solid line shows the linear regression best fit to the data given in (1).

relationship for solid needles of 20-80 μm tip diameter is consistent with the relationship developed from previous data from hollow microneedles of 60-160 μm tip diameter [22]. However, the slope of 0.00012 in (1) is less steep than the slope of 0.00019 determined in the previous study. This difference may be due to the geometric and mechanical differences between the solid tip of the polymer needles used here and the hollow tip of the metal needles used previously, although the relatively large error bars of the data may render this difference in slope insignificant.

E. Mechanical Analysis of Axial Failure Force of Polymer Microneedles

In addition to minimizing insertion force, microneedles should also maximize failure force to assure skin penetration without breaking. We first considered microneedle failure by buckling during axial loading as a function of microneedle length, base diameter, and Young's modulus.

Experimental measurements showed that failure force decreased with increasing microneedle length from 0.22 N for a 700-μm needle to 0.1 N for a 1500-μm needle (with an otherwise fixed geometry of a 25-μm tip and a 200-μm base diameter), as shown in Fig. 7(a). This approximately inversely proportional dependence of failure force with microneedle length constrains microneedles to relatively small dimensions or aspect ratios. Nonetheless, the insertion force required for microneedles used in Fig. 7(a) was 0.058 N (see (1)), which is 3.8-fold smaller than the fracture force for the 700-μm needle and 1.7-fold smaller than the 1500-μm needle. Thus, all of these microneedles are expected to insert into skin without failure.

Fig. 7(b) shows that failure force increased with increasing microneedle base diameter in a nonlinear manner. In each case, however, the failure force remained greater than the insertion force. Fig. 7(c) shows that failure force increased with increasing Young's modulus in an approximately linear manner. Young's modulus was varied by changing the polymer formulation used to make the microneedles. The weakest microneedle (i.e., Young's modulus of 1 GPa) had a failure force similar to the insertion force, indicating that this microneedle would not reliably insert into skin without breaking. The other polymer

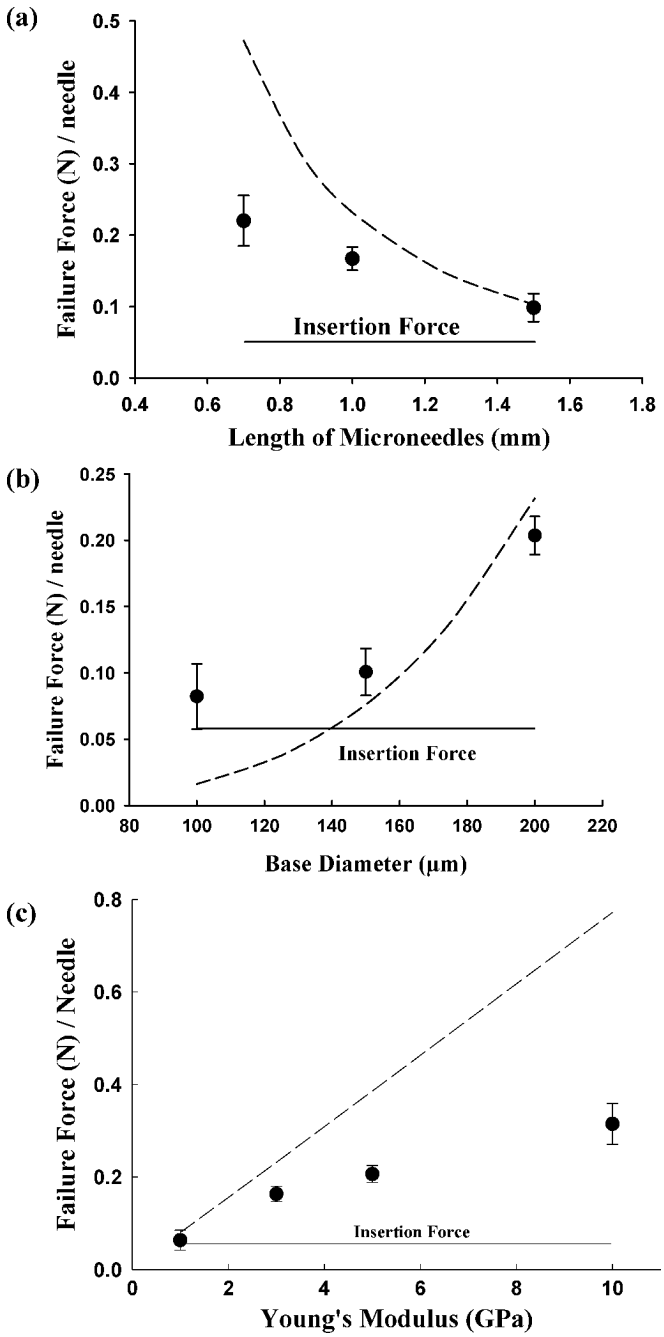

Fig. 7. Relationship between microneedle axial failure force and (a) microneedle length (for microneedles made of PLGA with 25-μm tip diameter and 200-μm base diameter), (b) microneedle base diameter (for microneedles made of PLGA with 25-μm tip diameter and 700 μm length, and (c) microneedle polymer Young's modulus (for microneedles with 25-μm tip diameter, 200-μm base diameter, and 1000-μm length). Young's modulus, E, and yield strength, S_z, were varied by making microneedles out of different polymers: PGA (E $\approx$ 10 GPa, $S_z \approx$ 90 MPa), PLA (E $\approx$ 5 GPa, $S_z \approx$ 70 MPa), high molecular weight PLGA (E $\approx$ 3 GPa, $S_z \approx$ 50 MPa), and low molecular weight PLGA (E $\approx$ 1 GPa, $S_z \approx$ 20 MPa). Mean values and standard deviation error bars are shown from n = 5–7 replicate experiments. The dashed lines indicate theoretical predictions of axial failure force using (2). The solid lines indicate insertion forces determined using (1).

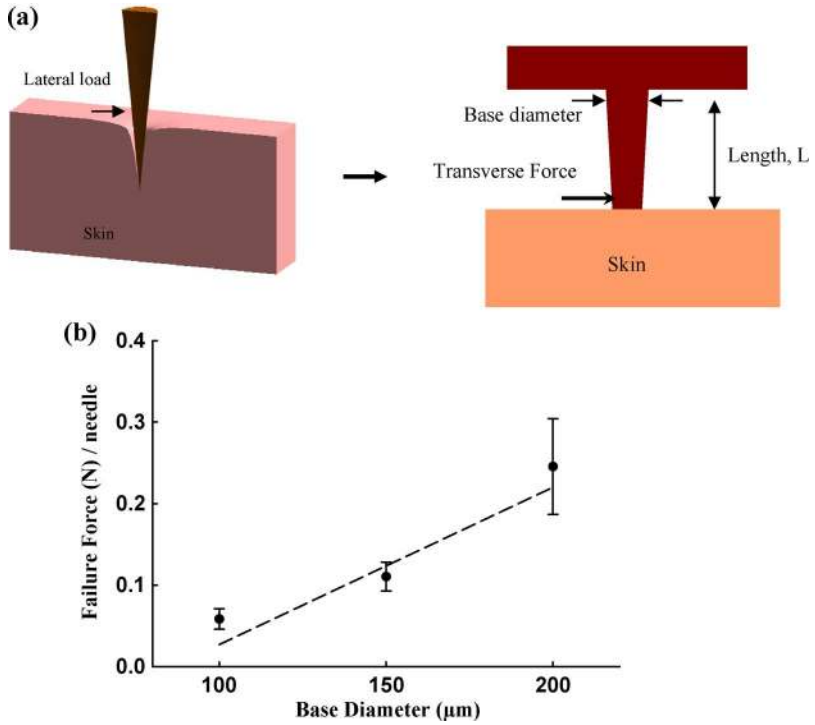

Fig. 8. Microneedle transverse failure force. (a) Schematic diagrams showing how skin deformation around a microneedle during insertion can generate a transverse force on the microneedle. (b) Microneedle transverse failure force as a function of base diameter for microneedles made of PGA with 25-μm tip diameter and 1000-μm length. Mean values and standard deviation error bars are shown from $\mathrm{n} = 5$ replicate experiments. The dashed line indicates theoretical predictions of transverse failure force using (4).

microneedles had failure forces at least two-fold greater than the insertion force. These findings are consistent with failure force measurements made previously for polymer microneedles [18].

As a companion to experimental measurements, we developed an analytical solution to predict microneedle failure based on failure due to buckling caused by elastic instability of the structure. For this analysis, we assumed that the base end of the microneedle was fixed in space, whereas the tip end was free to displace vertically and to rotate. Using an energy balance method developed previously for failure of a linearly tapered cone, the critical buckling force $(\mathrm{P_{cr}})$ is shown in (2) at the bottom of the page [26], where E is Young's modulus of the polymer, L is the length of the microneedle, $\mathrm{R_1}$ is the needle radius at $\mathrm{z} = 0$ and $\mathrm{R_2}$ is the radius at $\mathrm{z} = \mathrm{L}$.

Predictions from this theoretical analysis are shown in Fig. 7 as dashed lines. Overall, there is qualitative agreement between experimental and theoretical values and trends, but quantitatively the predictions tend to overpredict failure force. More specifically, in Fig. 7(a), a shorter column tended to fail at a load less than predicted by (2), which may be because shorter columns are more likely to fail by compression without appreciable buckling [27], which is not accounted for in the model. In Fig. 7(c), the weaker than predicted dependence of failure force on Young's modulus could be explained by creep buckling behavior (as opposed to elastic buckling anticipated by the model), due to the viscoelastic properties of the polymers [28], and differences in actual end fixity, due to different friction coefficients for different polymers [29].

F. Mechanical Analysis of Transverse Failure Force of Polymer Microneedles

We next considered microneedle failure during transverse loading as a function of microneedle base diameter. Although microneedles might ideally insert with a completely axial force, during actual insertion microneedles could experience a bending moment generated by a transverse tip force due to misalignment and deformation of the skin, as shown schematically in Fig. 8(a). Prior to and during insertion of microneedles, the skin has been shown to be significantly deformed by even more than half the length of the microneedle [30]. For this reason, failure by transverse loading should be considered.

$$P_{cr} = E\left(120\left(R_2\left(R_2^2(R_2-2R_1)+2R_1^3\right)-R_1^4\right) + \frac{\pi^2\left(20\left(R_2\left(R_2^2(-R_2+R_1)-R_1^3\right)+R_1^4\right)+\pi^2\left(R_2\left(R_2\left(R_2(R_2+R_1)+R_1^2+R_1^3\right)+R_1^4\right)\right)\right)}{(80\pi L^2)} \quad (2)$$

As a model system, a transverse force was applied to the distal half (i.e., the 500 μm closest to the tip) of a 1000-μm-long PGA microneedle, which simulated a 50% skin deflection before needle penetration. As shown in Fig. 8(b), failure force increased as base diameter was varied from 100 to 200 μm.

To theoretically analyze these date, we assumed that Hooke's law is valid, a transverse load is applied to half of the microneedle by the flexible skin, and that the geometry of the part of needle to which the transverse force is applied (i.e., the part away from the skin) is cylindrical. The maximum bending stress, σ, can then be expressed as [27]

$$\sigma = \frac{M(z) \cdot c}{I(z)} \tag{3}$$

where c is the distance from the centroidal axis to the outermost edge of the microneedle, $M(z)$ is the bending moment, and $I(z)$ is the moment of inertia of the cross section. By replacing the bending moment with the tip force, $\mathrm{F_t}$, multiplied by the needle length, L, the maximum transverse tip force that the needle can support is [13]

$$F_t = \frac{S_z \cdot I(z)}{c \cdot L} \tag{4}$$

where $\mathrm{S_z}$ is the yield strength of material. Predictions using (4) exhibit good agreement with experimental data, as shown in Fig. 8(b).

G. Imaging Polymer Microneedle Insertion Into Skin

Using the fabrication tools and the mechanical analysis developed in this study, we prepared three different microneedle designs for insertion into skin without failure. We first prepared short microneedles designed to insert just across the skin's epidermis. This needle was made of L-PLA, measuring 350 μm in length, 80 μm in diameter at the base, and 10 μm at the tip. L-PLA and the relatively large base diameter were selected to increase failure force, the sharp tip was selected to decrease insertion force, and the relatively short length was selected to limit penetration depth into the skin. As shown in Fig. 9(a), these microneedles penetrated approximately 100 μm into porcine cadaver skin. Delivery to this depth might be ideally suited for vaccines to target the highly immunogenic Langerhans cells found at the base of the epidermis. The microneedle insertion depth was smaller than the microneedle length because the skin deforms during microneedle insertion into skin [22], [30]. In this case, the 350 μm microneedle penetrated approximately 100 μm into the skin and caused an approximately 250 μm deformation of the skin surface.

We next prepared longer microneedles designed to insert into the upper dermis. These needles were made of L-PLA, measuring 750 μm in length, 150 μm in diameter at the base, and 10 μm at the tip. For this design, the larger base provided additional strength to compensate for the longer needle length. The integrated lens technique permitted fabrication of a very sharp tip even on such a long needle. As shown in Fig. 9(b), these microneedles penetrated 200–300 μm deep into the skin. Delivery at this depth may be ideal for delivery to the rich capillary bed found in the superficial dermis for rapid uptake into the circulation for systemic delivery.

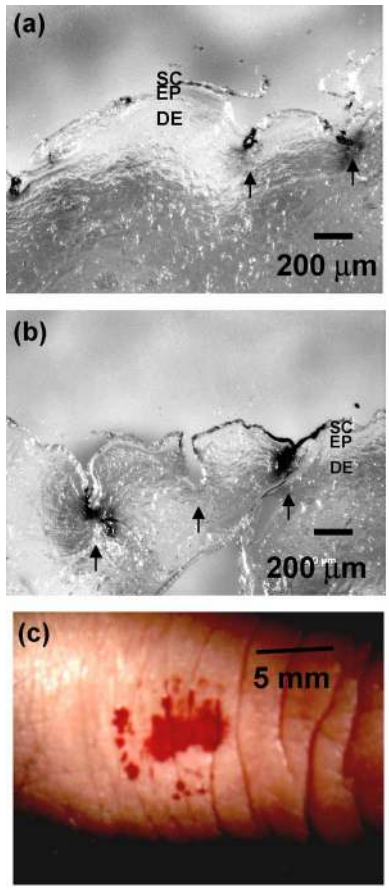

Fig. 9. Polymer microneedle insertion into the skin imaged by brightfield microscopy. (a) Histological sections showing staining sites of microneedle insertion into porcine cadaver skin using (a) a 350-μm-long microneedle (made of L-PLA with a 80-μm base diameter and 10-μm tip diameter) and (b) a 750-μm-long microneedle (made of L-PLA with a 150-μm base diameter and 10-μm tip diameter) (SC=stratum corneum, EP=epidermis, DE=dermis). (c) Surface image of the finger of a human subject showing blood on the skin surface produced by piercing with a 200-needle array of 1500-μm-long microneedles (made of PGA with a 250 μm base diameter and 10-μm tip diameter). In all cases, the microneedles showed minimal or no deformation after insertion into skin in these experiments (data not shown).

As a final test, we wanted to insert an array of microneedles into the skin of a human subject. To facilitate analysis, we designed very long microneedles that could pierce deeply enough to draw blood, which would validate that the needles inserted into the skin. These needles were made of PGA, measuring 1500 μm in length, 250 μm in diameter at the base, and 20 μm at the tip. Using a 200-microneedle array, these relatively long microneedles were strong enough to insert into the skin without buckling, as shown by the blood extracted from the skin in Fig. 9(c).

IV. Conclusion

Biodegradable polymer microneedles provide an attractive delivery method for current and emerging biopharmaceuticals, but improved microneedle fabrication and design are needed to create polymer microneedles with sufficient mechanical strength and simple manufacturing. To address these needs,

an integrated lens technique was developed, which produced tapered microneedle structures with high aspect ratios. Microneedle geometries could be predicted using ray-tracing techniques and controlled by selecting the geometry of the microlens and lens opening size. Various geometries of biodegradable polymer microneedles were created using a subsequent micromolding step.

Concerning microneedle mechanics, the force of microneedle insertion into the skin of human subjects was found to increase as a linear function of microneedle tip area, ranging from 0.037 to 0.6 N per needle for microneedles with tip diameters of 20 to 80 μm. Microneedle failure force by axial loading was found to increase with increasing base diameter, increasing Young's modulus, and decreasing needle length. Experimental values showed qualitative agreement with theoretical calculations, but theory generally overpredicted failure forces probably by not accounting for the viscoelastic behavior of polymers. In most cases, measured failure forces were at least two-fold greater than insertion forces, which indicates that these polymer microneedles insert into skin without breaking. Microneedle failure force by transverse loading caused by deformed skin was found to increase linearly with microneedle base diameter, which was in good agreement with theoretical modeling.

To test predicted mechanical behavior, microneedle designs having three different needle lengths were prepared and inserted into the skin of a porcine cadaver and a living human subject. By keeping needle tips sharp, using polymers with large Young's modulus, and increasing base diameter to compensate for the mechanical instability of longer needle length, microneedles ranging in length from 350 to 1500 μm were inserted into skin and demonstrated to selectively penetrate just across the epidermis, into the superficial dermis, and into the deeper dermis. Altogether, this study provides a versatile method to fabricate microneedles with geometrical and mechanical properties suitable to insert into skin for transdermal drug delivery.

ACKNOWLEDGMENT

The authors would like to thank R. E. Guldberg, H. Gill, S. Davis, J.-W. Park, and R. Kamath of the Georgia Institute of Technology for valuable technical discussion. This work was carried out in the Center for Drug Design, Development and Delivery, the Institute for Bioengineering and Bioscience, and the Microelectronics Research Center at Georgia Tech.

REFERENCES

[1] G. Walsh, "Biopharmaceuticals: Recent approvals and likely directions," *Trends Biotechnol.*, vol. 23, pp. 553–558, 2005.

[2] M. R. Prausnitz, S. Mitragotri, and R. Langer, "Current status and future potential of transdermal drug delivery," *Nat. Rev. Drug. Discov.*, vol. 3, pp. 115–124, 2004.

[3] Y. W. Chien, *Transdermal Controlled Systemic Medications*. New York: Markel Dekker, 1987.

[4] D. V. McAllister, M. G. Allen, and M. R. Prausnitz, "Microfabricated microneedles for gene and drug delivery," *Annu. Rev. Biomed. Eng.*, vol. 2, pp. 289–313, 2000.

[5] M. R. Prausnitz, "Microneedles for transdermal drug delivery," *Adv. Drug Deliv. Rev.*, vol. 56, pp. 581–587, 2004.

[6] M. L. Reed and W. K. Lye, "Microsystems for drug and gene delivery," *Proc. IEEE*, vol. 92, no. 1, pp. 56–75, Jan. 2004.

[7] W. Martanto, S. P. Davis, N. Holiday, J. Wang, H. Gill, and M. R. Prausnitz, "Transdermal delivery of insulin using microneedles *in vivo*," *Pharm. Res.*, vol. 21, pp. 947–952, 2004.

[8] M. Cormier, B. Johnson, M. Ameri, K. Nyam, L. Libiran, D. D. Zhang, and P. Daddona, "Transdermal delivery of desmopressin using a coated microneedle array patch system," *J. Control. Release*, vol. 97, pp. 503–511, 2004.

[9] W. Lin, M. Cormier, A. Samiee, A. Griffin, B. Johnson, C. L. Teng, G. E. Hardee, and P. E. Daddona, "Transdermal delivery of antisense oligonucleotides with microprojection patch (Macroflux) technology," *Pharm. Res.*, vol. 18, pp. 1789–1793, 2001.

[10] J. A. Mikszta, J. B. Alarcon, J. M. Brittingham, and D. E. Sutter, "Improved genetic immunization via micromechanical disruption of skin-barrier function and targeted epidermal delivery," *Nat. Med.*, vol. 8, pp. 415–419, 2002.

[11] S. Kaushik, A. H. Hord, D. D. Denson, D. V. McAllister, S. Smitra, M. G. Allen, and M. R. Prausnitz, "Lack of pain associated with microfabricated microneedles," *Anesth. Analg.*, vol. 92, pp. 502–504, 2001.

[12] S. Henry, D. V. McAllister, M. G. Allen, and M. R. Prausnitz, "Microfabricated microneedles: A novel approach to transdermal drug delivery," *J. Pharm. Sci.*, vol. 87, pp. 922–925, 1998.

[13] J. D. Zahn, N. H. Talbot, A. P. Pisano, and D. Liepmann, "Microfabricated polysilicon microneedles for minimally invasive biomedical devices," *Biomed. Microdevices*, vol. 2, pp. 295–303, 2000.

[14] J. G. E. Gardeniers, R. Luttge, A. Van der Berg, J. W. Berenschot, M. J. de Boer, Y. Yeshurun, M. Hefetz, and R. van't Oever, "Silicon micromachined hollow microneedles for transdermal liquid transport," *J. Microelectromech. Syst.*, vol. 6, pp. 855–862, 2003.

[15] J. Brazzle, I. Papautsky, and A. B. Frazier, "Micromachined needle arrays for drug delivery or fluid extraction," *IEEE Eng. Med. Biol. Mag.*, vol. 18, no. 6, pp. 53–58, Nov.-Dec. 1999.

[16] J. A. Matriano, M. Cormier, J. Johnson, W. A. Young, M. Buttery, K. Nyam, and P. E. Daddona, "Macroflux microprojection array patch technology: A new and efficient approach for intracutaneous immunization," *Pharm. Res.*, vol. 19, pp. 63–70, 2002.

[17] S. P. Davis, W. Martanto, M. G. Allen, and M. R. Prausnitz, "Hollow metal microneedles for insulin delivery to diabetic rats," *IEEE Trans. Biomed. Eng.*, vol. 52, no. 5, pp. 909–915, May 2005.

[18] J. H. Park, M. G. Allen, and M. R. Prausnitz, "Biodegradable polymer microneedles: Fabrication, mechanics and transdermal drug delivery," *J. Control. Release*, vol. 104, pp. 51–66, 2005.

[19] ——, "Polymer microneedles for controlled-release drug delivery," *Pharm. Res.*, vol. 23, pp. 1008–1019, 2006.

[20] M. Prausnitz, J. Mikszta, and J. Raeder-Devens, "Microneedles," in *Percutaneous Penetration Enhancers*, E. Smith and H. Maibach, Eds. Boca Raton, FL: CRC Press, 2005, pp. 239–255.

[21] J. H. Park, Y. K. Yoon, M. G. Allen, and M. R. Prausnitz, "High-aspect-ratio tapered structures using an integrated lens technique," presented at the IEEE MEMS 2004 Conference, Maastricht, Netherlands, 2004.

[22] S. P. Davis, B. J. Landis, Z. H. Adams, M. G. Allen, and M. R. Prausnitz, "Insertion of microneedles into skin: Measurement and prediction of insertion force and needle fracture force," *J. Biomech.*, vol. 37, pp. 1155–1163, 2004.

[23] M. R. Prausnitz, "The effects of electric current applied to skin: A review for transdermal drug delivery," *Adv. Drug. Deliv. Rev.*, vol. 18, pp. 395–425, 1996.

[24] H. Becker, K. Lowack, and A. Manz, "Planar quartz chips with submicron channels for two-dimensional capillary electrophoresis applications," *J. Micromech. Microeng.*, vol. 8, pp. 24–28, 1998.

[25] Y. K. Yoon, J. H. Park, F. Cros, and M. G. Allen, "Integrated vertical screen microfilter system using inclined SU-8 structures," presented at the IEEE 2003 MEMS Conference, Kyoto, Japan, 2003.

[26] W. G. Smith, "Analytical solutions for tapered column buckling," *Comput. Struct.*, vol. 28, pp. 677–681, 1988.

[27] R. L. Mott, *Applied Strength of Materials*. Upper Saddle River, NJ: Prentice-Hall, 1996.

[28] A. M. Vinogradov, "Buckling of viscoelastic beam columns," *AIAA J.*, vol. 25, pp. 479–483, 1987.

[29] W. F. Riley, L. D. Sturges, and D. H. Morris, *Mechanics of Materials*, W. F. Riley, L. D. Sturges, and D. H. Morris, Eds. New York: Wiley, 1999, pp. 568–578.

[30] W. Martanto, J. S. Moore, T. Couse, and M. R. Prausnitz, "Mechanism of fluid infusion during microneedle insertion and retraction," *J. Control. Release*, vol. 112, pp. 357–361, 2006.

Jung-Hwan Park received the B.S. degree in chemical engineering from Han-Yang University, Seoul, Korea, in 1990. He received the M.Sc. degree in chemical engineering from the Korea Advanced Institute of Technology, Taejon, Korea, in 1992. He received the Ph.D. degree in biomedical engineering from the Georgia Institute of Technology, Atlanta, in 2004.

He was a Research Scientist with the Research Institute of LG Chemical Corp., Taejon, from February, 1992 to July, 1997. He has worked as a Postdoctoral Fellow at the Georgia Institute of Technology. In March 2007, he joined Kyungwon University in Korea as an Assistant Professor in the Department of BioNano Technology. His current research interests include biomedical systems for the lab-on-a-chip, microdevices for drug delivery and 3-D microfabrication technology for biomedical application.

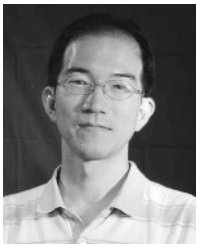

Yong-Kyu Yoon (S'03–M'04) received the B.S. and M.S. degrees in electrical engineering from the Seoul National University, Seoul, Korea. He received the M.S.E.E. degree from the New Jersey Institute of Technology, Newark, in 1999 and the Ph.D. degree in electrical and computer engineering from the Georgia Institute of Technology, Atlanta, in 2004.

After graduation, he was a Postdoctoral Fellow with the Microelectronics Research Center of Georgia Institute of Technology. In August 2006, he joined the State University of New York at Buffalo as an Assistant Professor in the Electrical Engineering Department. His current research interests include 3-D MEMS technology; design and implementation of low GHz RF components, millimeter-wave antennas, and waveguides; bio/microfluidic systems for the lab-on-a-chip; nanofabrication and its bio/chemical applications; microsensors and actuators; electronic and MEMS packaging; and ferroelectric material study and its RF/optical applications.

Seong-O Choi received the B.S. degree in physics in 1998 from Yonsei University, Seoul, Korea. He received the M.S. degree in biomedical engineering from University of Southern California, Los Angeles, in 2001 and the M.S. degree in electrical and computer engineering from Georgia Institute of Technology, Atlanta, in 2003. He is currently working toward the Ph.D. degree in electrical and computer engineering at Georgia Institute of Technology.

His research focuses on development of 3-D microfabrication technology utilizing micromolding and its applications to biomedical microsystems including electrically active microneedle array for electroporation and 3-D microelectrode array for neural recording/stimulation. His other interests are in microfluidic systems for biomedical applications, and in fabrication technology for polymer-based microsystems.

Mark R. Prausnitz received the B.S. degree from Stanford University, Stanford, CA, in 1988 and the Ph.D. degree from the Massachusetts Institute of Technology, Cambridge, in 1994, both in the field of chemical engineering.

He is currently Professor of Chemical and Biomedical Engineering and the Emerson Lewis Faculty Fellow at the Georgia Institute of Technology, Atlanta. He also serves as the Director of the Center for Drug Design, Development and Delivery at the Georgia Institute of Technology. He previously worked as a Biomedical Engineer for ORBIS International, a Junior Chemical Engineer at ALZA Corporation, and an Instructor of technical communication at Stanford University. His research interests address the application of engineering tools to solve drug, gene and vaccine delivery problems, especially in the context of microfabricated devices for transdermal drug and vaccine delivery and ultrasound-based mechanisms for intracellular delivery of drugs and genes.

Prof. Prausnitz has received a number of awards, including the Curtis W. McGraw Research Award from the American Society for Engineering Education (2004), the CAREER Young Investigator Award from the National Science Foundation (1996), and the Young Investigator Award (2005) and Outstanding Pharmaceutical Paper Award (1992) from the Controlled Release Society. In 2002, he served as the NSF/NIH Scholar-in-Residence at the National Institutes of Health.

Mark G. Allen (M'89–SM'04) received the B.A. degree in chemistry, the B.S.E. degree in chemical engineering, and the B.S.E. degree in electrical engineering from the University of Pennsylvania, Philadelphia, and the S.M. and Ph.D. degrees from the Massachusetts Institute of Technology, Cambridge.

In 1989, he joined the faculty of the School of Electrical and Computer Engineering of the Georgia Institute of Technology, Atlanta, where he is currently Regents' Professor and holds the J.M. Pettit Professorship in Microelectronics. His current research interests are in the field of microfabrication and nanofabrication technology, with emphasis on new approaches to fabricate devices with characteristic lengths in the micro- to nanoscale from both silicon and nonsilicon materials. Examples include micromagnetics, high temperature sensors, small-scale power generation, biofluidic microvasculatures and implantable microsensors, and the use of microstructures to create nanostructures.

Dr. Allen served as the Co-Chair of the 1996 IEEE Microelectromechanical Systems Conference.